43rd AIAA Aerospace Sciences Meeting and Exhibit, 10-13 Jan 2005, Reno, Nevada

Improved De-icing of an Inclined Windshield Surface

Haribalan Kumar* and Subrata Roy†
Computational Plasma Dynamics Laboratory, Kettering University, Flint, Michigan 48504

The removal of ice from the vehicle windshield is necessary to ensure adequate driver visibility. The presence of more than one phase and the complex interaction of fluid thermal processes necessitate an efficient numerical simulation for its complete understanding and optimization. We present a deicing simulation for a three-dimensional shield-cabin assembly. Jets issuing from a defroster nozzle flushed at the bottom of this cabin impinge upon the inclined glass surface. Steady state heat transfer analysis for varying flow and heat transfer characteristics inside this geometry was reported earlier. Here the unsteady process of defrosting on the windshield is investigated using solidification and melting model. The main goal of the paper is to study the melting process and to arrive at an effective design based on traditional control parameters like jet impingement angles for minimum defrosting time. Correlations for defrosting as functions of Nusselt number and impingement angle have been found.

Nomenclature

C_p	Specific heat at constant pressure, kJ/kg-K
E	Specific enthalpy, kJ/kg
H	Convection heat transfer coefficient, W/m^{2}K
k	Thermal conductivity, W/m-K
Nu	Nusselt number
P	Static pressure, Pa
S_L	Source term (latent heat)
t	Time, sec
T	Temperature, K
u_i	i-th component of velocity, m/s
V	Jet velocity, m/s
x_i	Spatial coordinates, m

Greek symbols

∇	Spatial gradient, m^{-1}
λ	Liquid fraction
Λ	Latent heat, kJ
μ	Viscosity, N-s/m^2
ρ	Density, kg/m^3
κ	Permeability

Subscripts

Avg	Average
Eff	Effective
in	Inlet (at nozzle exit)
i,j	Direction of spatial derivatives
L	Liquidus
m	Mush
Ref	Reference
s	Slip between ice and water
S	Solidus
w	Wall

* Graduate Research Assistant, 1700 West Third Ave, kuma6164@kettering.edu and AIAA Student Member
† Associate Professor of Mechanical Engineering, 1700 West Third Ave, sroy@kettering.edu, AIAA Associate Fellow

I. Introduction

The application of jet impingement heat transfer for defrosting and defogging automotive and aircraft systems has gained considerable interest in recent years. De-icing or defrosting is a two-phase fluid thermal process for removal of ice from a surface through a process of melting. For the windshield of a transport vehicle, melting has to be achieved in the quickest possible way to ensure driver visibility and passenger safety. In a traditional defroster arrangement, a simple electric fan pushes hot air into a gap between the top of the blower ductwork and the top panels of dashboard trim. Several slots have been cut into the trim panel, separated by directional vanes. These vanes control the left-right angle between the plane of the windshield and the incoming warm air. This arrangement relies on convection to transfer heat from air to glass and on conduction from windshield to the layer of ice atop it making the process conjugate in nature. As shown in Figure 1, the heat flux necessary for melting the ice is carried through a path of resistance across the cabin-shield and shield-ice interface giving rise to a combination of conduction and convection resistances. The effectiveness of heat transfer also depends on flow parameters like the Reynolds number and wall shear, thickness of glass and the thermal properties of ice and glass and heat loss from ice due to ambient conditions outside the control volume. Thus understanding these heat transfer characteristics is vital for better optimizing the melting process.

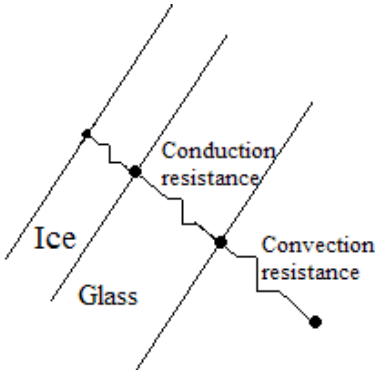

Figure 1. Heat transfer resistance path

Several basic experimental and numerical studies of impinging air jets have been reported on a flat surface over the past three decades [1-8]. Some of the computational efforts were focused on modeling heat transfer without phase change. Several researchers have also studied the deicing patterns over the windshield [7-9] and aircraft wings [10]. These reports range from a patent on fluidic oscillators for better flow and heat transfer patterns [7] to the theoretical prediction and computation of ice formation [11]. Automotive engineers have applied commercial software like Fluent, ICEM-CFD and Star-CD [8,9] to predict and validate the melting of ice over the windshield.

The importance of design parameters as affecting the performance of a defroster was studied recently [5,6]. These parameters include flow angles, nozzle dimension and location and nozzle configuration (rectangular or circular). For a defroster, an optimum choice of jet speed and inlet blower temperature has to be made as a compromise between power, cost and the melting time. An effective design may be the one that has the maximum melting characteristic for a given blower power. Thus, establishing a correlation for defrosting as functions of time, flow and heat transfer parameters, and impingement angles can be an important contribution in obtaining an improved design.

In this vein, Roy and Patel [6] have investigated the effect of Reynolds number (Re) and impingement angles on local and average Nusselt number (Nu), turbulence intensity and wall y^+. The analysis was done at steady state with constant blower temperature. Here, we have investigated the unsteady two phase defrosting process due to a pair of jets impinging upon an inclined surface. Based on practical data, the jet temperature is varied with time. The intention is to identify correlation functions that will enable efficient design of windshield defrosters. As far as we know, this is the first time such analyses are reported based on design considerations.

Figure 2 shows the jet, the inclined plane and its associated cabin volume used for this study. The cabin is bounded by the top, side and back walls. The jets ensue from two rectangular openings (each 0.019m×0.241m) in the bottom wall and impinge upon the inclined surface made of glass with thickness 6mm. The rectangular openings are centered on the bottom wall with a gap of 0.127m between them. The directional vanes in the nozzle control the streamwise (ϕ) and sweep (β) angles of flow. A thin sheet of 0.4mm thickness initially filled with ice is attached to the outer layer of the shield. The target plane is

inclined at an angle of 39°. The temperature of the air jets vary based on the blower data plotted in Figure 3.. This provides the source of heat required to melt the ice.

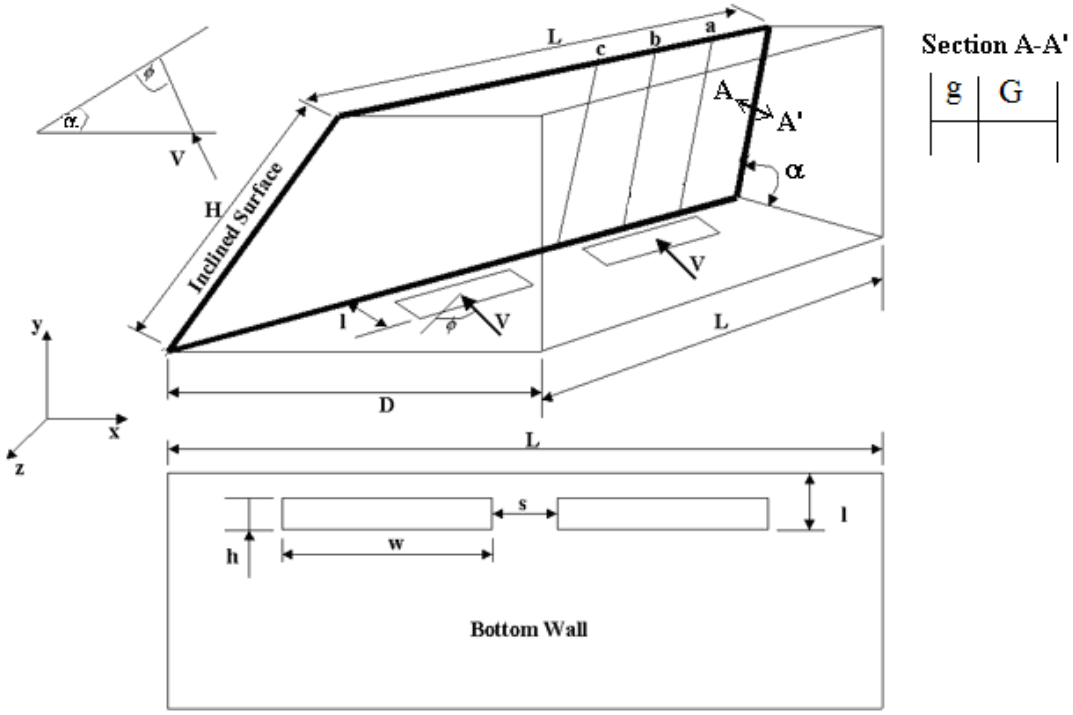

Length of Inclined surface, L	1.447 m
Width of inclined surface, H	0.719 m
Surface inclination angle, α	39°
Shield surface thickness, G	0.006 m
Ice layer thickness, g	0.0004 m
Location of nozzle, l	0.134 m
Length of nozzle exit plane, h	0.019 m
Width of nozzle exit plane, w	0.241 m
Jet impingement angle, ϕ (on x-y plane)	21° – 66°
Cross-wise angle, β (on y-z plane)	0°, 5°, 10°
Span of bottom wall, D	0.896 m
Distance between nozzle exit planes, s	0.127 m

Figure 2: Schematic of computational domain of the windshield and the associated cabin volume.

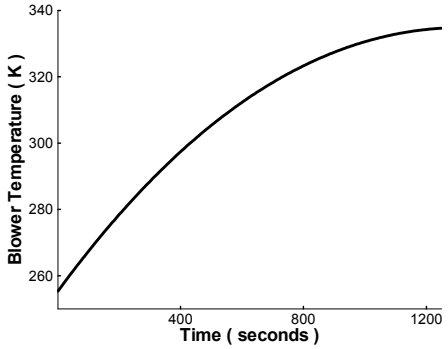

Figure 3. Blower temperature curve plotted as a function of time.

The mean velocity of the jet is chosen to be 8m/s. The corresponding flow Reynolds number is 20000, based on the hydraulic diameter of the rectangular opening. The impingement angle ϕ is varied from 21° to 66° in steps of 15° in the xy-plane. For each ϕ, the sweep angle β is varied from 0° to 10° in steps of 5° in the outward direction in the yz-plane. The jet openings are in plane with the bottom floor for all these experiments making the floor jet injection angle ($180°-\phi-\beta$) to vary between 75° and 120°. The impingement point of the jet on the inclined shield is $(l-h/2)(\cos\alpha+\sin\alpha/\tan\phi)$ from the crotch. Two correlations are established – one between jet impingement angles and melting characteristics of ice and the average nusselt number evolution during defrosting.

II. Theoretical Formulation

The problem of defrosting is formulated using a two-step process. Airflow inside the cabin is analyzed at steady state. The flow is turbulent and renormalized group (RNG) two-equation k-ε turbulence model [12] is employed. The continuity and momentum equations are as given in Ref. [6]. Once steady state solutions are obtained, the unsteady process of melting is simulated. Conjugate heat transfer calculations are done between air, windshield and ice for the time varying jet temperature while maintaining the air velocity profiles steady. The energy equation solved for this step is given as

$$\frac{\partial(\rho E)}{\partial t}+\frac{\partial(\rho u_i E)}{\partial x_i}=k\frac{\partial T^2}{\partial x_i^2}+S_L \tag{1}$$

where E is enthalpy, ρ is the density, u_j is the air velocity components, k is the thermal conductivity and S_L is the source term discussed below. The following two-phase enthalpy- porosity formulation is used to model the melting of ice on the outer surface.

$$E=\left(E_{ref}+\int_{T_{ref}}^{T}c_p dT\right)+\Delta E \tag{2}$$

The reference enthalpy E_{ref} is chosen to be 298 kJ/kg. The first term in (2) is the sensible heat. $\Delta E = \lambda\Lambda$ is the latent heat content which varies from zero to Λ determined by liquid fraction, λ

$$\lambda=\frac{T-T_S}{T_L-T_S},\ 0\le\lambda\le 1 \tag{3}$$

The ice is treated as a mushy region. The source term in (1) is defined based on the Carman-Koseny equation [13]

$$S_L=C_m\frac{(1-\lambda)^2}{\lambda^3+\varepsilon}\left(u_{m,i}-u_{s,i}\right) \tag{4}$$

where C_m is the mushy zone constant (~10^5), which measures the amplitude of damping and ε is a small number (~10^{-3}) used to prevent division by zero. The mush velocity is computed using Darcy law $u_{m,i}=-(\kappa/\mu)\nabla P$. We have considered negligible slip velocity ($u_{s,i}$) between solid and melting zones and thus ignored the relative velocity between the solid ice and melted mush. Through a process of iteration between Eqns. (1), (2) and (4), the liquid fraction λ in (3) is updated at each step following Ref. [14].

Table 1 lists all the material properties and reference temperatures used for solving the two-phase conjugate heat transfer.

Glass	ρ=2500 kg/m^3, C_p=0.750 kJ/kg-K, k=1.4 W/m-K
Ice	ρ=920 kg/m^3, C_p=2.040 kJ/kg-K, k=1.88 W/m-K, Λ = 334.96 kJ/kg, T_S = 271 K, T_L = 273 K, μ=0.00553 N-s/m^2
Air	ρ=1.225 kg/m^3, C_p=1.00643 kJ/kg, k=0.0242 W/m-K, μ=1.789e-05 N-s/m^2

Table 1: Material Properties

III. Numerical Details

The fluid-thermal processes in the computational domain are investigated by using a finite volume based commercial code Fluent6.1.22©. The details of the flow code are given earlier [5,6]. For inlet surface of nozzle has hydraulic

diameter of 0.035m with turbulence intensity of 10%. The temperature of the blower as a function of time is defined by curve in Figure 3. The outlet at the back wall has a hydraulic diameter of 0.612m. The backflow turbulence intensity is given as 10% while a backflow temperature of 273 K is assumed. The top, side and bottom wall (excluding the two defroster openings) are considered adiabatic. Fluent treats the walls appearing between a fluid and a solid region as a coupled surface. The solution is calculated directly from the solution in adjacent cell. It is assumed that the outside temperature is same as that of ice and the ambient air velocity is negligible. Hence there is no convective heat loss from ice. The fluid and heat transfer equations are solved on a computational mesh of 216319 elements inside the cabin created using T-Grid meshing scheme. The choice of this element length is based on earlier mesh independent studies done on a similar model [6]. The glass and ice layers are filled with 18432 and 6912 hexagonal elements, respectively. The system of equations is solved using implicit Gauss-Seidal in conjunction with Algebraic Multi-Grid method.

The iteration is considered to have converged when the solution residual for continuity and momentum equations become less than 10^{-4} and 10^{-7} for the energy equation.

IV. Results and Discussion

The windshield is considered as "cleared" or "defrosted" when it conforms to SAE J902 standards. Figure 4 shows two important regions A and C on the windshield for which the acceptable defrosted minima are recommended in the standard [15]. For the model under consideration, the shortest distance from P to eye was measured as 0.6m, the eye E is 0.3m away from the side of the vehicle and the height H from the manikin H-point with driver seat in rearmost position to the eye is 0.635 m. The automotive requirement for defrosting in Table 2 shows that while all of region C needs to be cleared, region A may not require the total removal of ice.

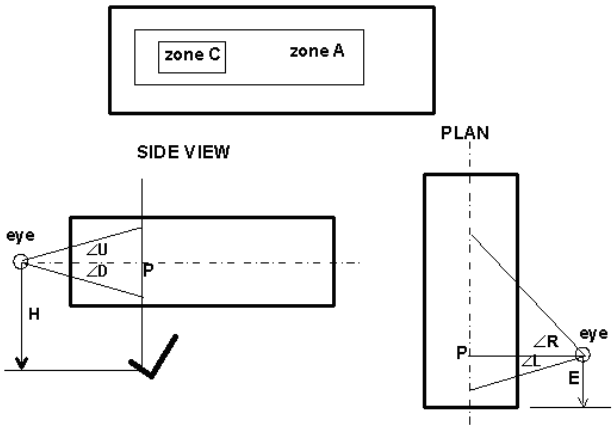

Figure 4. SAEJ902 standard for windshield clearing [11]

Zone	Minimum %	Angle L (degrees)	Angle R (degrees)	Angle U (degrees)	Angle D (degrees)
A	80	18	56	10	5
C	100	10	15	5	1

Table 2. SAEJ902 standard zones for defrosting in 30 minutes

Figures 5 through 13 discuss results of the simulated cases. The percentage of zones A and C that are cleared in 20 minutes is documented in Table 3. The best and worst performances of deicing are highlighted in bold. For jet angles $\phi = 51°$ and $\beta = 10°$, all ice melts in regions A (99%) and C (100%). Hereafter, this is referred to as the best arrangement. The worst occurs for $\phi = 21°$ and $\beta = 0°$ where only 29% of C and 62% of A defrosts within 20 minutes. Hereafter, we refer to this case as the worst arrangement. Figure 5 plots the liquid fraction (λ) distribution on the windshield surface at four different time stations, namely 400s, 600s, 900s and 1200s. At 400 seconds only 2.3% of the ice is melted at two impingement regions, by the time it reaches 600 seconds 85.7% of the ice about the impingement regions is melted. Interestingly, the jets issued from rectangular slots with high aspect ratios create near circular footprints on the windshield. Ice completely melts in the C region and nearly 98.8% for the region A within 20 minutes. The stipulated driver visibility conditions are reached in 15 minutes.

ϕ (deg)	β (deg)	% of A melted in 1200sec	% of C melted in 1200 sec	
66	0	87	82	
	5	91	99	
	10	90	93	
51	0	84	75	
	5	93.5	100	
	10	**99**	**100**	← Best
36	0	77	64	
	5	88.4	85.7	
	10	95	100	
21	**0**	**62**	**28.5**	← Worst
	5	71	50	
	10	68	57	

Table 3: Twelve simulation cases tested for various jet angles.

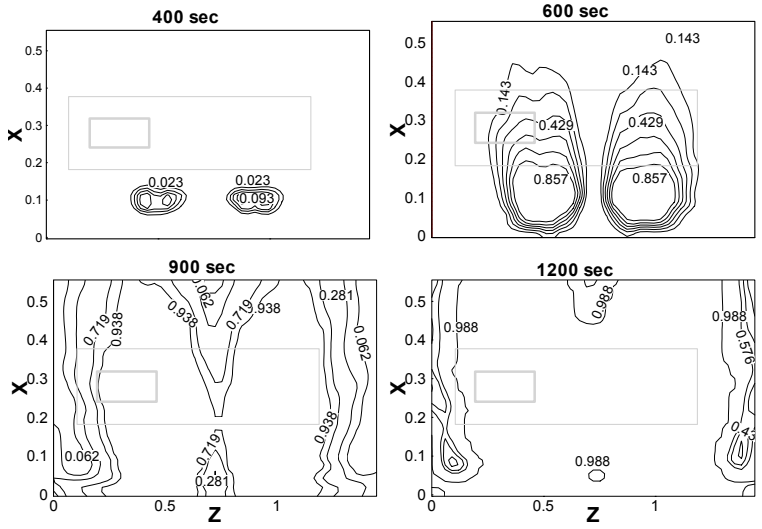

Figure 5. Time evolution of liquid fraction contour for the best arrangement.

In comparison, Figure 6 shows contours of λ at 600s, 700s, 900s and 1200s for the worst arrangement. While for the best arrangement it takes about 400s for the ice to start melting, no significant melting starts before 600s for the worst arrangement. After 20 minutes only the central region upstream of flow melts, keeping half of regions A and C frozen. The major flow without adequate attachment to the shield carries away the unutilized heat. There is hardly any melting near the crotch because of negligible minor flow region below the impingement zone. For better understanding of melting characteristic, solid fraction after 20 minutes is plotted on lines a and c (as shown in Fig. 1) for two impingement angles ($\phi = 21°$ and $36°$) and three sweep angles ($\beta = 0°$, $5°$ and $10°$) are shown in Figure 7.

The impingement angle ϕ has significant impact on melting along the selected lines a and c. For line a, which is closest to the driver's vision, the melting characteristic improves as β increases. However, there is an inverse relation between β and the melting characteristic for line c, which is the furthest from the driver's eye. This is obvious as line c lies between the stagnation zones. Line b is exactly on the impingement zone and there is not much effect of β on the defrosting. Note that complete melting occurs for ϕ=36^o along line b (not shown).

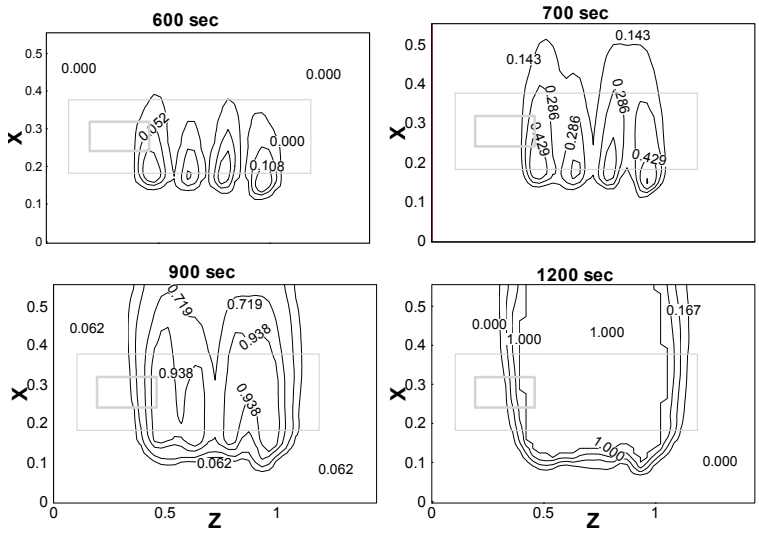

Figure 6. Time evolution of liquid fraction contour for the worst arrangement.

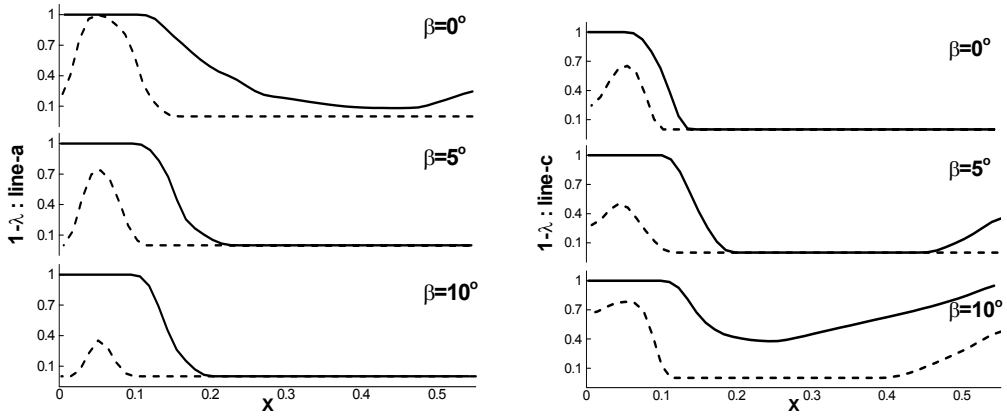

Figure 7. Solid fraction at 1200 sec. Solid line represents ϕ=21° and dotted line represents ϕ=36°.

Figure 8 summarizes the average liquid fraction, $\lambda_{avg} = \left(\int_A \lambda \, dA\right) \Big/ A$, on the windshield area for twelve test cases given in Table 3. The following three correlations are established using quadratic polynomial fit from the computed solution data for $0° \le \beta \le 10°$ and $0° \le \phi \le 75°$.

(1) For β = 0°, $\lambda_{avg} = -0.48\phi^2 + 1.22\phi + 0.02$

(2) For β = 5°, $\lambda_{avg} = -0.95\phi^2 + 1.97\phi - 0.15$

(3) For β = 10°, $\lambda_{avg} = -1.4\phi^2 + 2.64\phi - 0.31$

We avoided the power fit representation of the data as that will fail to indicate the optimum operating range, $50° \le \phi \le 60°$.

Figures 9 and 10 demonstrate the enthalpy contour on the outer surface of the windshield for the best and worst arrangements. The enthalpy around impingement zone increases sharply between 300 and 600 seconds from 12 kJ/kg to 323 kJ/kg and reaches a peak of 415 kJ/kg at 1200 seconds in Figure 9. The enthalpy is indicative of temperature distribution on shield as can be seen from Eqn. (2). The transition of enthalpy across the shield from impingement zone to boundaries is smooth signifying transfer of heat flux in all directions on the inclined surface. The predicted enthalpy distribution for the worst arrangement in Figure 10 also shows a gradual increase in enthalpy from 10 kJ/kg to 395 kJ/kg. As compared to the best case, temperature distribution is localized signifying inefficient heat transfer. The average enthalpy of the best arrangement is nearly twice than that of the worst. It is also observed that nearly 45 kJ/kg of air is added as sensible heat

content in 20 minutes as against nearly 30 kJ/kg for the worst arrangement. Hence the best blower vane design configuration offers the least resistance to heat flux compared to all the 12 cases considered.

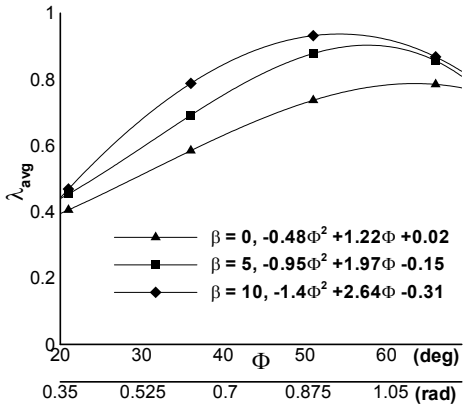

Figure 8. Average liquid fraction over the windshield–curve-fit has ϕ in radians.

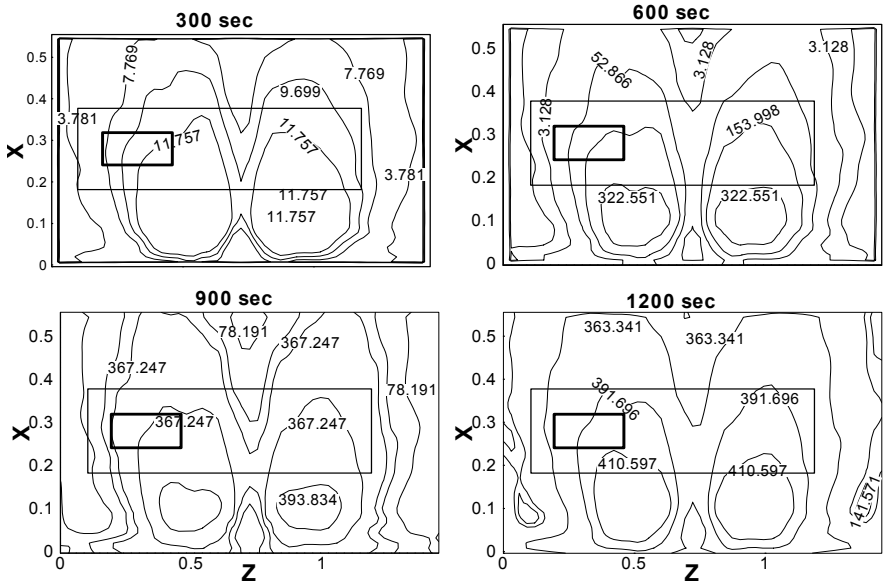

Figure 9. Time evolution of the total enthalpy distribution for the best arrangement.

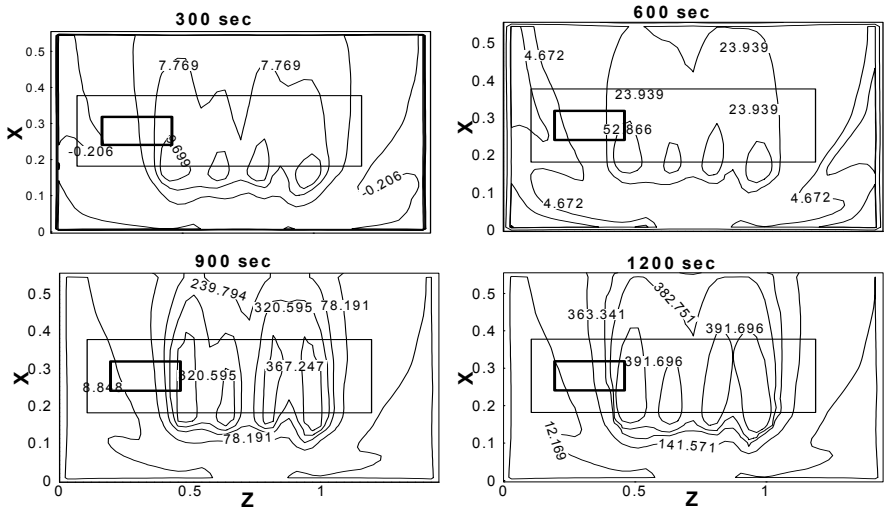

Figure 10. Time evolution of the total enthalpy distribution for the worst arrangement

Figures 11 through 13 plot the Nusselt number distribution for the windshield, which is exposed to impinging jets. Figure 11 shows the time evolution for best arrangement with Nu ranging from 4 to 12. Clearly, maximum heat transfer happens about jet impingement points. For the worst arrangement, the nusselt number distribution shows fingerlike patterns near the impingement region in Figure 12 similar to the liquid fraction (Fig. 6) and enthalpy (Fig. 10) distributions. The peak nusselt number after 20 minutes is only a quarter of that in Fig. 11. It is the fluid-thermal interaction described in Ref. [6] that may cause these patches and, in effect, poor heat transfer. For this, acute impingement angles of $\phi = 21°$ and $\beta = 0°$, the jet attaches the upper lip of the windshield and does not get enough contact with glass to inject heat carried by the blower air.

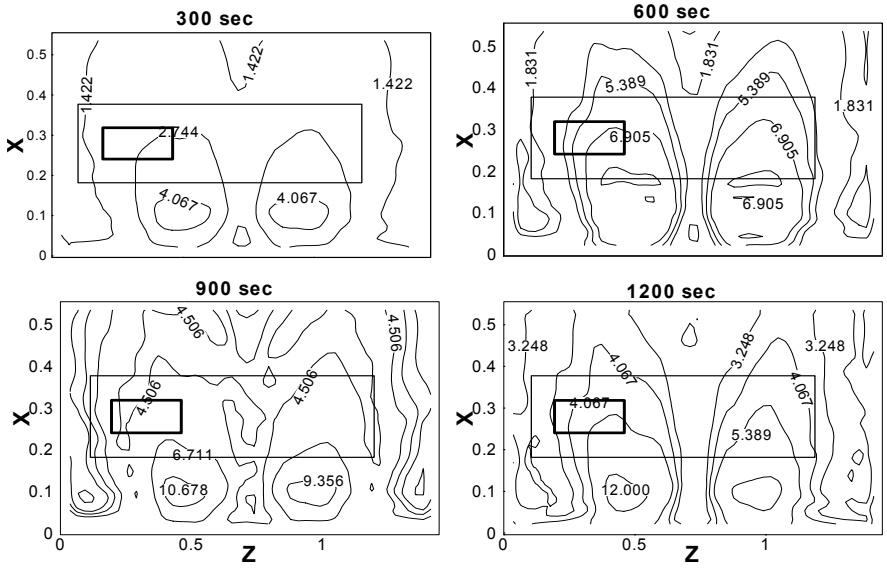

Figure 11. Nusselt number on the inner surface for the best arrangement.

The area averaged non-dimensional heat transfer coefficient, $\mathrm{Nu}_{avg} = \left(\int_{Area} \mathrm{Nu}\, dA\right) \Big/ A$, is plotted in Figure 13 as a function of time for the best and the worst configurations. Interestingly, the average nusselt number peaks at about 900 sec for both cases. However, at the nusselt number peak, the best jet arrangement with $\mathrm{Nu}_{avg} \approx 5$ is about 2.5 times more effective in transferring heat as compared to the worst arrangement with $\mathrm{Nu}_{avg} \approx 2$. The decrease in slope of curve after around 900 sec may be attributed to the nature of the driving blower temperature profile, which flattens around that time decreasing the rate of input power supplied to the control volume. Hence, growth rate of convected heat transfer to shield decreases resulting in the depicted behavior of Nu_{avg}. For $200s \le t \le 1200s$, the correlations for these two arrangements are found as follows:

(1) Best configuration, $\phi = 51°$ and $\beta = 10°$, $Nu_{avg} = -8.1\times10^{-6}t^2 + 1.45\times10^{-2}t - 1.32$

(2) Worst configuration, $\phi = 21°$ and $\beta = 0°$, $Nu_{avg} = -3\times10^{-6}t^2 + 5.37\times10^{-3}t - 0.31$

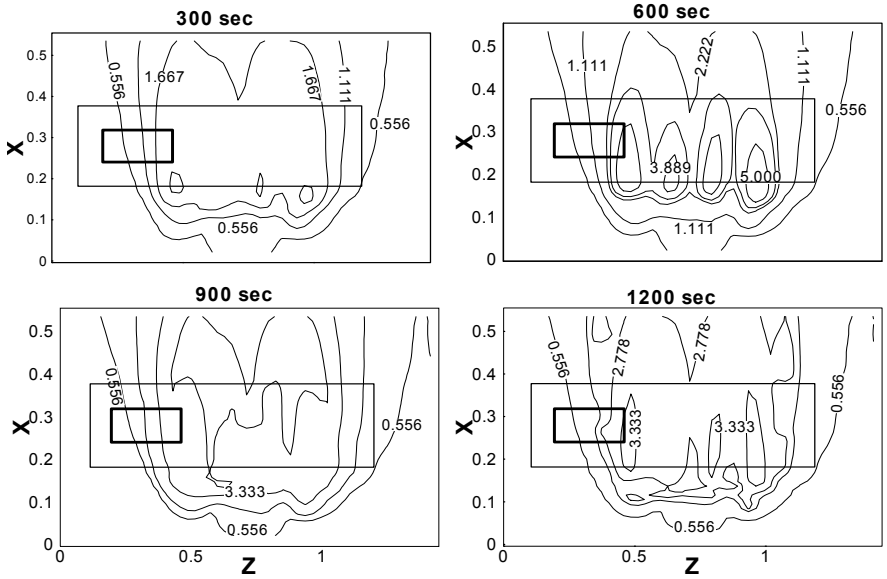

Figure 12. Nusselt number on the inner surface for the worst arrangement

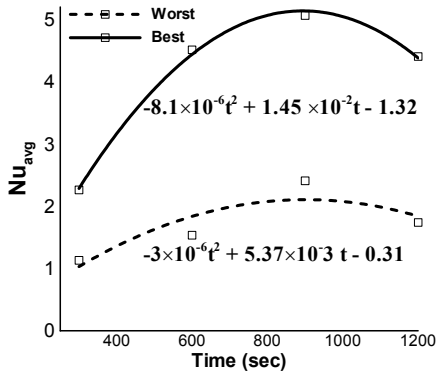

Figure 13. Average Nusselt number on the inner surface of the windshield

V. Conclusions

We present a deicing simulation for a realistic vehicle windshield inside which hot air jets impinge upon a flat inclined glass surface with a layer of ice on the other side. The presence of heterogeneous phases in equilibrium and the complex interaction of fluid thermal processes necessitate an efficient numerical simulation for its complete understanding and optimization. Here the unsteady process of melting of ice on the windshield is investigated using solidification and melting model, which relates enthalpy and porosity of ice, treated as mushy zone. The main goal of the paper is to compare the control parameters like impingement and sweep angle for minimization of defrosting time for a given ice and glass thickness. Parameters like enthalpy and nusselt number are used to understand the heat transfer process. The best and worst possible designs are suggested. Correlations have been found for defrosting and heat transfer parameters. The methodology can be utilized to understand the deicing phenomenon in aircraft wings and shield. A comparative test using other viable alternatives deicing methods of deicing are also being attempted.

VI. References

[1]H. Martin, Heat and mass transfer between impinging gas jets and solid surfaces, Advances in Heat Transfer, vol. 13, Academic Press, New York, 1977, pp. 1–60.
[2]S. Polat, B. Huang, A.S. Mujumdar and W.J.M. Douglas, Numerical flow and heat transfer under impinging jets: a review, Ann. Rev. Numer. Fluid Mech. Heat Transfer 2, 157–197 (1989).
[3]R.J. Goldstein and M.E. Franchett, Heat transfer from a flat surface to an oblique impinging jet, ASME J. Heat Transfer 110, 84–90 (1988).
[4]L. Huang and M.S. El-Genk, Heat transfer of an impinging jet on a flat surface, Int. J. Heat Mass Transfer 37 (13), 1915–1923 (1994).
[5]S. Roy, K. Nasr, P. Patel and B. AbdoulNour, An experimental and numerical study of heat transfer off an inclined plane surface subject to an impingement airflow, Intl. Journal of Heat and Mass Transfer, 45, 1615-1629 (2002).
[6]S. Roy and P. Patel, Study of heat transfer for a pair of rectangular jets impinging on an inclined surface, International Journal of Heat and Mass Transfer, 46, 411-425 (2003).
[7]Stouffer and Sharkitt, Air sweep defroster, US Patent no. 464485, 1987.
[8]A. Aroussi, A Hassan and Y.S. Morsi, Numerical simulation of the airflow over and heat transfer through a vehicle windshield defrosting and demisting, Heat and Mass Transfer 39, 401-405 (2003).
[9]J. G. Lee, Y. Jiang, J. Przekwas and M. Sioshansi, Validation of Computational vehicle windshield de-icing with comparison test data, SAE 971833, 1997
[10]A. Farag and Lin-Jie Huang, CFD Analysis and Validation of Automotive Windshield De-icing Simulation, (2003) SAE International, 2003-01-1079.
[11]R.W. Gent, N.P. Dart and J.T. Cansdale, Aircraft icing, Phil. Trans. Royal Soc. Lond. A 358, 2873-2911 (2000).
[12]S.H. Lam, On the RNG theory of turbulence, Phys. Fluids A 4, 1007-1017 (1992).
[13]V.R. Voller and C. Prakash, A fixed grid numerical modeling methodology for convection-diffusion mushy region phase-change problems, International Journal of Heat and Mass Transfer, 30, 1709-1719 (1987).
[14]V.R. Voller and C.R. Swaminathan, A general source-Based method for solidification phase change, Numer. Heat Transfer B, 19(2), 175-189 (1991).
[15]Surface vehicle recommended practice-Passenger Car Windshield Defrosting Systems; SAE J902, Rev. JUL 2003.